RSC Advances

Synthesis and characterization of geometrically tunable nano-size hollow silicate particles and their dip-coating prepared films for thermal management applications

Journal:	*RSC Advances*
Manuscript ID	RA-ART-09-2015-018267.R1
Article Type:	Paper
Date Submitted by the Author:	28-Oct-2015
Complete List of Authors:	Virtudazo, Raymond; National Institute of Materials Science, Global Research Center for Environment and Energy Based on Nanomaterials Science Lin, Ye; Shenyang Jianzhu University, School of Municipal and Environmental Engineering Wu, Rudder; National Institute of Materials Science,
Subject area & keyword:	Materials & nanotechnology < Energy

RSC Advances

ARTICLE

Synthesis and characterization of geometrically tunable nano-size hollow silicate particles and their dip-coating prepared films for thermal management applications

Received 00th January 20xx,
Accepted 00th January 20xx

DOI: 10.1039/x0xx00000x

www.rsc.org/

Raymond V.Rivera Virtudazo[a], Ye Lin[b] and Rudder T. Wu*[c]

The synthesis of geometrically tunable nano-size hollow silicate particles (NHSPs) using water-based poly_(methacrylic acid) sodium salt (NaPMA) colloidal nano size-aggregate particles as soft-templates, tetraethyl orthosilicate (TEOS) as a silica precursor and ammonia hydroxide (NH_4OH) as a catalyst by simple sol-gel reaction was carried out. Tuning the nano-size diameter of NHSPs between 60 nm and 200 nm and decreasing the shell thickness from 40 nm down to 18 nm were achieved by only varying the concentrations of alternative-NaPMA and the amount of TEOS, respectively. The thermal insulating feature of NHSPs was demonstrated by coating the glass substrate with NHSPs, a reduction of approximately 29.9 % in thermal conductivity was observed after coating the glass substrate, which was evaluated by contactless approach using the Xenon flash lamp set-up. The coated-glass with NHSPs was prepared by simple sequential adsorption of poly_(allylamine hydroxide) (PAH) followed by deposition of NHSPs on the cleaned glass substrate surfaces using an automated dip coater. The dip coated samples showed good thermal insulating properties as well as good transparency in the visible light range .

Introduction

Intense research efforts have been placed on porous-hollow silicate particles, due to their unique properties such us hollow inner volume, large surface area, low thermal conductivity, low density and good bio-compatibility.[1, 2] Consequently, many research groups have attempted and reported various preparations of multi-functional porous-hollow silicate particles for practical applications such as nano-containers for drug delivery, [2-4] as supporting materials for catalysts,[4] thermal insulators for heat management[5, 6] and light fillers for nano-composite materials. [2, 7, 8]

Porous-hollow particles have been regarded as promising (filler) materials for thermal management with respect to thermal insulation due to their pore-cavity with large amount of trapped gas. A good example is the commercially available heat insulation paint that used porous-hollow particles as fillers. Insulating walls and doors with porous-hollow particles helps prevent heat exchange between inside and outside of the building. [6, 9, 10]

Still, porous-hollow particle as (an additive in) insulators cannot be easily applied especially to transparent materials such as exterior glasses, windows and windscreen, because some have large size ranging from several hundreds of nanometers to several tens of micrometers which are opaque in the visible range.[6, 11, 12] It should be noted that the transparency of nano-objects dispersed within the matrices depends on the size, shape, refractive index, and the distribution state of nano-objects within the matrix. In terms of diameter-size, it is known that in order to be transparent in the visible range, the average size of porous-hollow particle should be as small as around several tens of nanometers; a phenomenon known as Mie scattering. [6, 9]

Currently, there are many synthetic routes to obtain small-size porous-hollow particle as being reported by several research groups.[3, 4, 7, 12] Some of them used metal/metal oxide nanoparticles, semiconductors nano-crystals,[3, 13, 14] block copolymers micelles, polymeric colloidal aggregates as templates to prepare porous-hollow particle in tens of nanometer-size diameter.[14, 15] To date, there have been some established procedures with respect to the assembly of porous-hollow particles to fabricate an insulating material. Most of them used the polymer matrix to form composite thin films. [16-18]

In contrast, our focus is to investigate porous-hollow silicate particle as an insulation material (aiming for transparency and

[a]*Global Research Center for Environment and Energy Based on Nanomaterials Science (GREEN), National Institute for Materials Science (NIMS), Namiki, Tsukuba, Ibaraki 305-0044 Japan*
[b]*School of Municipal and Environmental Engineering, Shenyang Jianzhu University, Shenyang China*
[c]*National Institute for Materials Science (NIMS),Tsukuba, Ibaraki 305-0044 Japan*
**corresponding author. TEL: +81-(0)29-860-4702 FAX: +81-(0)29-860-4984*
**E-mail: WU.rudder@nims.go.jp*

†Electronic Supplementary Information (ESI) available: Experimental details, detailed XRD graphs, ^{29}Si-NMR, EDX, thermogravimetric analysis, SEM, TEM, N_2 sorption, DFT graphs, BJH graphs, typical set-up of xenon flash method, sample thermal calculations and thermal conductivity graphs. See
DOI: 10.1039/x0xx00000x

heat-blocking property like composite thin layers) for building applications such as in window glasses.

In this paper, we aim to evaluate nano-size hollow silicate particles (NHSPs) prepared using an alternative water-soluble polymer (as soft template) for thermal insulation. Then we initially investigate (using Xenon flash method) the fabricated coated-glass composed of NHSPs for the application of thermal insulation. The xenon flash method is one of the several methods to measure thermo physical properties of solid materials. The simplicity of sample preparation, fast measurement and good accuracy are some of the advantages of this non-contact, non-destructive testing technique[19] which is good for samples that involves nano-coating.

Poly (methacrylic acid) sodium salt (NaPMA) was used as an alternative water-based polymer in order to form colloidal nano-aggregates (soft-template). Aside from that it is noted as non-harmful in water,[20] NaPMA is quite accessible commercially. This route is a good example in developing an environmentally benign synthesis using eco-friendly materials.

Here, we reported a simple process in attaining stable and scalable route in forming NHSPs with tunable sizes and shell thickness at room temperature. The synthesized NHSPs shows good physico-chemical properties, especially on the simplicity of the process in tuning the surface area property of the NHSPs, an ideal model for the formation NHSPs is drawn schematically in Fig. 1.

In addition, to verify the thermal insulation of the material, NHSPs were embedded onto the surface of the glass by forming a thin coating layer composed of NHSPs) using our modified dip coating process (Fig. S1†). The coated-glass with NHSPs shows good heat insulation properties with good transparency.

Experimental

Chemicals / Materials

Poly|(methacrylic acid) sodium salt (NaPMA, Sigma-Aldrich, Co., 40 weight percent (wt %) in aqueous solution, MW= 4,000~6,000), tetraethyl orthosilicate (TEOS, 98 % Sigma-Aldrich, Co.), poly (allylamine hydroxide) (PAH, Sigma-Aldrich, Co.), ammonium hydroxide (NH_4OH, 28% Sigma-Aldrich, Co.), sodium chloride (NaCl, Sigma-Aldrich, Co.), sodium hydroxide (NaOH, Wako Pure Chemical IND., Ltd., 5 mol L^{-1} in solution), ethanol (EtOH, 99 % Wako Pure Chemical Ind., Ltd.), Glass substrates (GS, Muto Pure Chemical Co., Ltd.).

Synthesis of core-shell nano size silicate particles

In this research, we adopted the procedure similar to the ones used by other groups[21-23] except that the core-templating agent used during the synthesis was an alternative soluble water-based polyelectrolyte solution combined with Stöber method.[23, 24]

Here, 0.22 g of NaPMA was dissolved in 2.5 mL of NH_4OH. Then, 50 mL of ethanol was added to the mixture, followed by the injection of five aliquots of TEOS totaling 1.00 mL (1 h time interval per drop) under vigorous magnetic stirring at room temperature.[23]

A white colloidal suspension was obtained after a 10 h aging

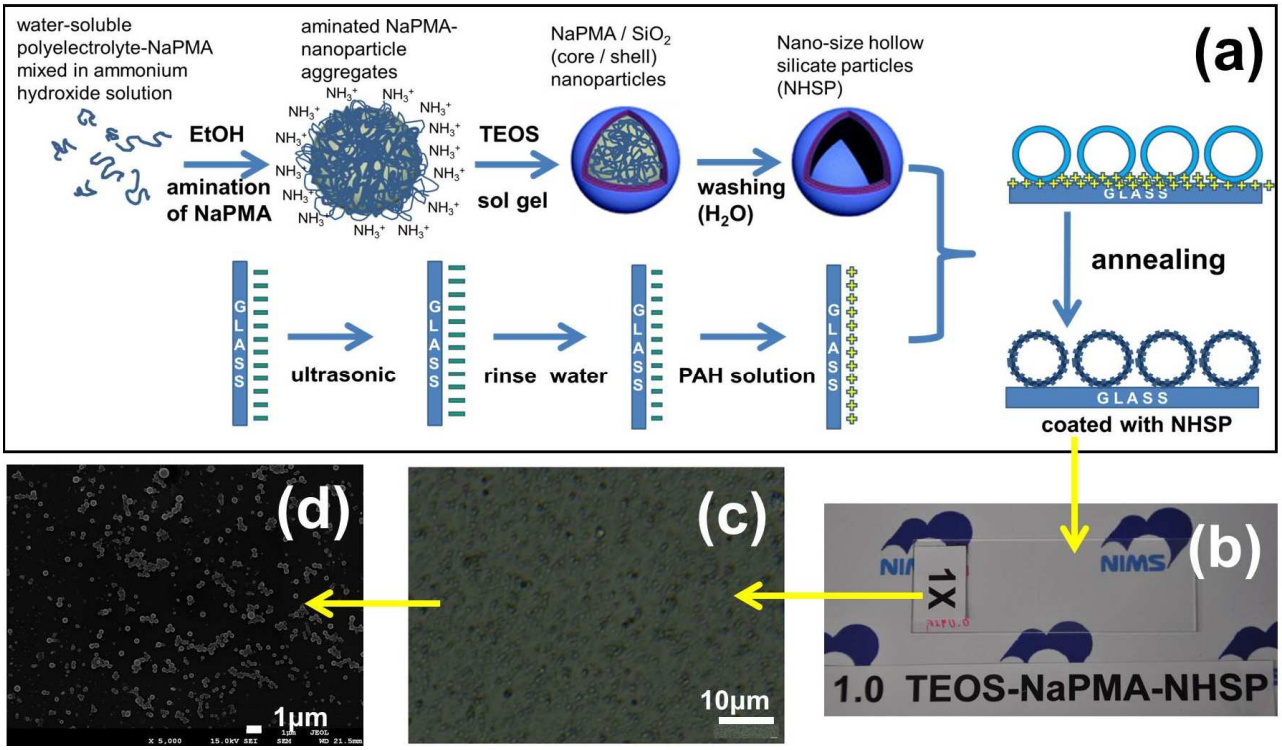

Fig. 1 (a, b) SEM images (transmission, T and secondary electron imaging mode, SE) of the (a-I, b-I) dried and (a-II, b-II) calcined powder of NHSPs in varying (a-I, a-II) X-TEOS and (b-I, b-II) Y-NaPMA concentrations. The (c, d) TEM images (c-III, d-III) high-magnification of (c-I, d-I) dried and (c-II, c-III, d-II, d-III) calcined-NHSPs samples with varying (c-I, c-II, c-III) X-TEOS and (d-I, d-II, d-III) Y-NaPMA concentrations.

period, which approximately contained 0.92 wt % of core-shell silicate particles (Fig. S2†). The enhancement of shell stability of NHSPs and the elimination of NH_4OH in the solution was done by stirring the solution in fume hood.

In order to observe the effect of the varied amount of silica sol and NaPMA-polymer concentrations, the amount of TEOS (mL) and NaPMA concentrations (mg mL^{-1}) were adjusted from 1.0 down to 0.20 mL and from 1.0 up to 5.5 mg mL^{-1}, respectively.

Fabrication of nano-size hollow silicate particles (NHSPs)

Subsequently, the milky white colloidal suspension was filtered, washed and re-dispersed with deionized water for the removal of water-based polymer, dried in vacuum oven at 120 °C for 24 h to yield NHSPs in powder form

Modified dip coating process

To fabricate coated-glass with NHSPs, sequential adsorption of PAH was followed by the deposition of NHSPs on the cleaned glass substrate surfaces using an automated dip coater (DT-0001-S1, SDI Co., Ltd.). A percentage solid concentration (wt % sc) of NHSP powder (varied from 0.1 wt % sc and 0.8 wt % sc.) was mixed in slightly acidic water (pH 4) and the mixture was subsequently stirred vigorously for at least 10 h. Slightly acidic water maintained at pH 4 [25] was used for all the solutions (i.e rinsed and washed) and for the duration of dipping process. The glass substrate was sonicated in 1.0 mol L^{-1} NaOH for 15 min and then rinsed in pH 4 solution for 15 min. The PAH solution was a mixture of PAH (10 mg), NaCl (16 mg) and water (10 mL, H_2O).[26] Clean glass substrate was first immersed in the PAH solution for 5 s prior to dip coating, then submerged in NHSPs solution for about 20 min before withdrawal followed by final rinsing in slightly acidic water (equivalent to one cycle of immersion: 1x). To maintain single layer, the withdrawal speed was kept at 0.3 mm s^{-1}.‡ After every dipping, initially the glass substrate with NHSPs was dried for 2 min at room temperature, before vacuum dry at 120 °C for 24 h to remove any residual solvent before annealing at the 400 °C for 2 h for densification of the coating. Then a simple process flow for the formation NHSPs and fabrication of coated-glass with NHSPs is also illustrated in Fig. 1 and Fig. S1†.

Characterization

X-ray diffraction (XRD). NHSPs were characterized by XRD (New D8 ADVANCE, Bruker) with Cu Kα radiation (λ=1.54056 Å), and at a scanning rate (2θ) of 0.05° s^{-1}, an operating voltage of 40 kV and an emission current 40 mA.

Thermogravimetric/differential thermal analysis (TG/DTA). The thermal analysis of the NHSPs was investigated using the automatic TG/DTA (DTG-60, Shimadzu Corp.). The temperature profile involves a heat rate of about 10 °C min^{-1} from 22 °C up to 700 °C in air atmosphere.

Scanning electron microscopy (SEM). Surface morphology of hollow particles was done by SEM equipped with energy dispersive x-ray spectroscopy (EDX) using JSM-7001F (JEOL Corp.); S-4800-EDX (Hitachi Corp.) and SU-8000 (Hitachi Corp.). The working voltage was 15 kV.

High resolution-transmission electron microscopy (HR-TEM). Detailed surface morphology and microstructure of hollow particles were examined using HR-TEM equipped with EDX using JEM-2100F (JEOL Corp.). The usual working voltage was 200 kV. Prior to the examination of SEM and TEM observation, NHSPs samples were first dispersed in ethanol ultrasonically and a drop of this suspension was applied to the copper grid coated with carbon film.

Digital optical microscope (OM). OM images were recorded by VHX series (Keyence Corp.) used for the surface observation of the coated-glass with NHSPs.

Solid-sate ^{29}Si-nuclear magnetic-resonance (^{29}Si-NMR). For structural analysis, ^{29}Si-NMR at 6 kHz using JNM-ECA series FT NMR (JEOL Resonance Corp.) was used.

Particle size distribution (PSD). The average PSD with zeta potential was determined by nano-sizer-Delsa instruments (Delsa-NanoC, Beckman Coulter and Malvern Zetasizer, Malvern Instruments).

Ultraviolet-visible and near-infrared (UV-Vis-NIR) spectrophotometer. The transmittance and reflectance (optical properties) was determined by UV-Vis-NIR spectrometry (Jasco V-570, JASCO Corp.). The spectra were acquired over the range of 300 – 100 nm (visible range).

N_2 sorption. The specific surface area ($s.a_{BET}$) was calculated by the Brunauer-Emmett-Teller (BET)[27] then the average pore size distribution was both determined by density functional theory (DFT) method and Barrett-Joyner-Halenda (BJH) method [28] via an automatic surface area analyzer ($s.a_{BET}$; Autosorb iQ_2 Quantachrome instrument) using Nitrogen gas (N_2) adsorption and desorption isotherm recorded at 77 K. For more detailed pore-size distribution of the NHSPs, DFT method was used. It was noted that BJH method underestimates the diameter of pore-size distribution of NHSPs.[29] Total pore volume ($V_{t\text{-}BJH}$) was estimated from the amount adsorbed at a relative pressure of ~0.99.[27] All dried and calcined-NHSPs samples were degassed at 150 °C and 10^{-2} kPa pressure for 22 h prior to the surface area measurement.

Thermal conductivity analysis using Xenon flash lamp. The thermal conductivity was measured using a purpose-built Xenon flash lamp, a thermal characterization instrument.[19, 30] The coated-glass with NHSPs (dip coated film on one side of the glass substrate) was measured to evaluate the thermal conduction property. In enhancing light (heat) absorption and avoiding reflection, a black tape was applied on both sides of glass substrate samples. The light source is a Xenon flash lamp L7684 with a built-in reflector (Hamamatsu Photonics Co. Ltd.). The spectral distribution is 190 nm - 2000 nm, and the maximum average input is 1 J per single flash and 60 W for continuous flashing. The maximum flashing frequency is 60 *Hz* **‡‡.** Continuous flashing mode with the maximum intensity was used to heat up the sample. Thermocouples were fixed on two sides of a glass substrate to measure the temperature change. Real-time temperatures were monitored and recorded using tracking software KIDS (CHINO Corp.). The thickness of each sample before and after dip coating was measured carefully with an electronic caliper. Flash lamp continuously heated the sample until ΔT was steady to insure ΔT reached the saturated

state, where ΔT is the temperature difference between the back and the front surface of the sample. In this case, the measurement process of the heat flux was considered to be in steady state.

The Fourier's law is represented by the following equation.

$$q = \frac{k\mathrm{A}\Delta\mathrm{T}}{\Delta\mathrm{x}} \quad (1)$$

q and A represent the heat flux and the area receiving this heat flux, respectively.[31,32] The $\Delta\mathrm{T}$ represents the temperature difference, which is measured using thermocouples. While $\Delta\mathrm{x}$, refers to the thickness of a samples which was measured by an electronic caliper. Then, k refers to the thermal conductivity of a sample. Since the heat flux (q) was considered to be constant during all measurements, the following equations can be obtained.

$$q_G = q_{CG} \quad (2)$$

where, q_G and q_{CG} stand for heat flux of the glass and coated-glass, respectively. The area receiving heat flux in all cases was assumed to be the same; hence, Equation 2 can be further simplified, as shown below (Fig. S5 †).

$$k_{CG} = \frac{k_G \Delta\mathrm{x}_{\mathrm{CG}} \Delta\mathrm{T}_{\mathrm{G}}}{\Delta\mathrm{T}_{\mathrm{CG}} \Delta\mathrm{x}_{\mathrm{G}}} \quad (3)$$

The thermal conductivity of a coated-glass with NHSPs (k_{CG}) can therefore be calculated, wherein thermal conductivity of the glass (k_G), temperature difference of the glass ($\Delta\mathrm{T}_{\mathrm{G}}$), temperature difference of the coated-glass with NHSPs ($\Delta\mathrm{T}_{\mathrm{CG}}$), thickness of the coated-glass with NHSPs ($\Delta\mathrm{x}_{\mathrm{CG}}$) and thickness of the glass substrate ($\Delta\mathrm{x}_{\mathrm{G}}$) are known quantities.

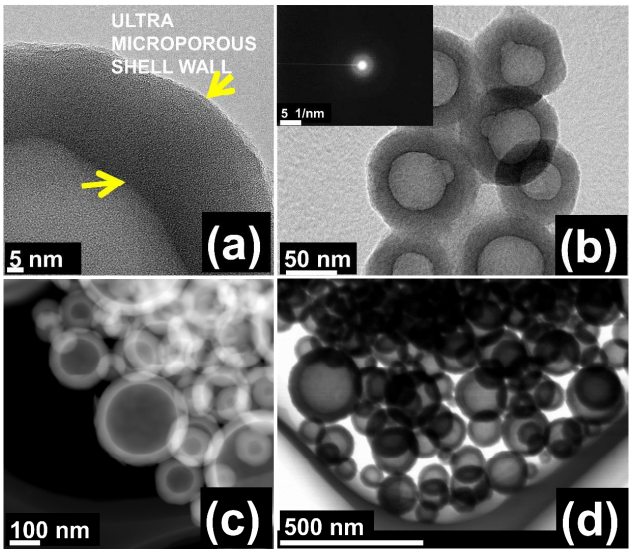

Fig. 2 TEM images of calcined (a) high-magnification image of NHSPs with ultra-microporous shell wall, (b) NHSPs with (inset) diffraction ring pattern, (c) typical morphological hollow shape of a calcined-NHSPs and (d) STEM image (transmission mode, T) of NHSPs after washing and drying.

Results and discussion

As shown in Fig. 1a, the water–soluble NaPMA–polyelectrolyte formed core nanoparticles (colloidal aggregates) in ethanol solution. Then, core-shell silicate nanoparticles were formed by the ammonia-catalyzed hydrolysis of TEOS. After then, the removal of core-NaPMA nanoparticles was done by washing (or calcination) for the formation of NHSPs. The interaction between animated carboxylic groups of core-NaPMA-(polyelectrolyte)-chains and silanol groups of silicate is the driving force for the formation of silicate shell (deposition of silicate sheets) onto the surface of the core-NaPMA-nanoparticles during the hydrolysis and condensation of TEOS.

As shown in Fig. 2, the hollow structure of NHSPs could be clearly observed in TEM and STEM. Furthermore, the ultra-microporous surface pattern was detected in the shell wall of the NHSPs using the high magnification TEM as shown in Fig. 2a. From this image, the amorphous phase silicate shell wall was confirmed through the ring diffraction pattern[33] as shown in Fig. 2b (inset). At this point, the overall hollow size inside-diameter corresponds to the dissolved water-soluble–NaPMA particles (core-template). The geometrical hollow shape and the thickness of the outer shell wall remain unchanged even after washing or calcination, a complete and hollow interior with ultra-microporous surface morphologies shell wall still exists as clearly shown in Fig. 2c. STEM image (Fig. 2d) of NHSPs confirmed that the particles were randomly distributed with uniformly nano-spherical shape. To demonstrate the tuning of the hollow nano-sizes and thickness of the NHSPs shell wall, we varied the amount of TEOS and NaPMA concentrations.

Effect of TEOS and NaPMA concentrations onto the NHSPs

A series of experimental samples were prepared to investigate the effect of TEOS and NaPMA concentrations on the synthesis of NHSPs. X-TEOS denotes varying amount of TEOS (X=1.0 – 0.25 mL) while the Y-NaPMA represents varying NaPMA concentrations (Y=1.0 – 5.5 mg mL^{-1}) ‡‡‡.

Based on XRD data shown in Figs. 3a and 3b, regardless whether the sample specimens were calcined or not and even if their perspective concentrations were varied, both X-TEOS (Fig. 3a) and Y-NaPMA (Fig. 3b) exhibited typical amorphous phase with broad peak pattern centered around 23° over the range of 2θ angles from 10° to 60° (Fig. S6 †). These patterns were basic characteristic for an amorphous silica pattern.[34] This collaborated to the diffraction ring pattern as shown in (inset) Fig. 2b. The existence of silica was further proved by the combined results of Si-NMR (see, Fig. S7a †) and EDX analysis (Fig. S7b †). The results verified the presence of the silicate structures and the main elemental component Si and O exist within the shell wall of NHSPs.

The critical weight loss of the NHSPs was investigated with varying X-TEOS and Y-NaPMA, by means of the thermal properties of the NHSPs after washing (see, Figs. S8, S9, and S10 †) using TG analysis. As shown in Figs. 3c-I and 3c-II wherein X-TEOS and Y-NaPMA were varied. Generally, there

were three main stages of weight-loss. The first percentage weight-loss below 150 °C (~12 %) was due to the evaporation of physically adsorbed water (H_2O) and residual solvent. The second percentage weight-loss occurs at 200–450 °C (~20 %) was directed to the decomposition of silica bonded groups, partial condensation of terminal silanol groups and the remaining organic substance (NaPMA), particularly at 300–400 °C. Finally, the third percentage weight-loss at above 500 °C was the final condensation of silanol groups that form siloxane bonds (~34 %).[35] As shown in the TG analysis, increasing Y-NaPMA clearly increased percentage weight-loss (Fig. 3c-II) while increasing X-TEOS decreased percentage weight-loss (Fig. 3c-I). From these primary results, it was evident that moderate increase of the silica content (X-TEOS) increased the production of hollow particles.[23] We also monitored the average particle size distribution with varying the amount of X-TEOS and Y-NaPMA concentrations. Nano-size analyzer was used to detect the average PSD for X-TEOS and Y-NaPMA. In Figs. 3d-I and 3d-II, this was presented as an average diameter size versus the increasing amount of X-TEOS or Y-NaPMA concentrations (Fig. S11 †). As shown in Fig. 3d-I, a graph showing the relationship between the amount of X-TEOS and the average nano-size diameter of NHSPs were observed. The graph showed that the average hollow nano-size particles remained constant around 120 nm to 140 nm even the X-TEOS increased. But in Fig. 3d-II, wherein the graph indicates the relationship between the amounts of Y-NaPMA versus the average nano-size diameter of NHSPs, revealed that the average hollow nano-size particles accelerated from 60 nm up to 180 nm as the concentrations of Y-NaPMA increased. Here, we can confer that the nano-size of NHSPs was manipulated by controlling the amount of NaPMA concentrations with constant (approximate) specific gravity (in solution, Figs. S2 and S11 †). These were verified through STEM and TEM images as shown in Fig. 4 (Figs. S12-S15 †).

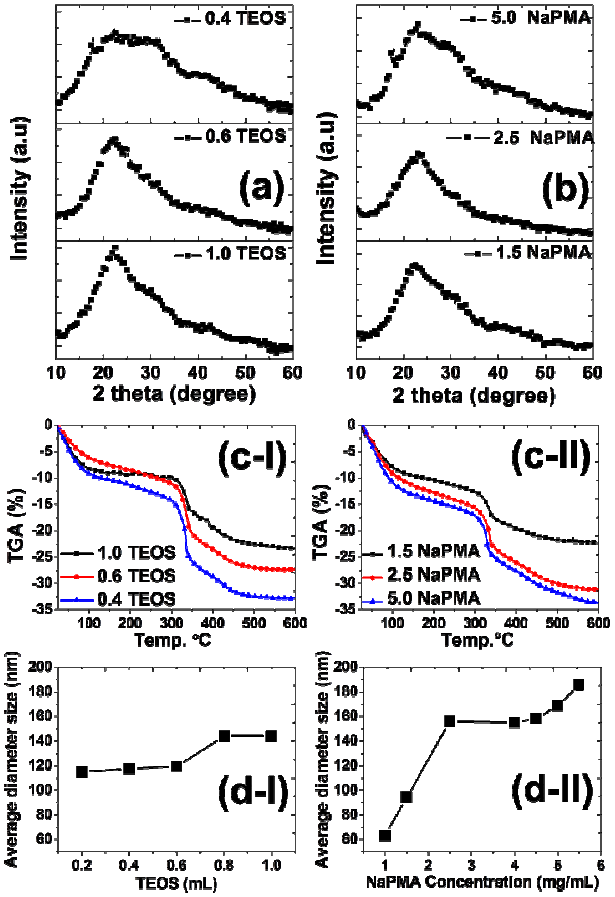

Fig. 3 (a, b) Amorphous X-ray diffraction spectra with varying (a) X-TEOS and (b) Y-NaPMA concentrations. In (c-I, c-II) thermogravimeteric analysis pattern and (d-I, d-II) average particle size distribution with varying (c-I, d-I) X-TEOS and (c-II, d-II) Y-NaPMA concentrations.

Based on the observed STEM and TEM images, the effect of varying the X-TEOS and Y-NaPMA was clearly revealed in Fig. 4. The images showed the stability of the nano-size hollow structures which matched on the observed particle size distribution graphs. With the increasing amount of X-TEOS (Fig. 4a), the nano-size diameter of NHSPs was approximately constant (see, Fig. S12 †). However, when Y-NaPMA (Fig. 4b) was varied, the observed average outer diameter of the NHSPs dramatically increased (see, Fig. S13 †). This was confirmed by the STEM images wherein the geometrical shape-stability of the dried NHSPs (Figs. 4a-I and 4b-I) and even after the calcination of the NHSPs (Figs. 4a-II and 4b-II) remains unaffected. These were also proven base on the transmission mode (T) as shown in Figs. 4a and 4b, all the samples revealed a hollow cavity upon varying the amount of X-TEOS and Y-NaPMA concentrations.

In detecting the detailed surface shell morphology of NHSPs, the TEM images were helpful in observing the effect of varying the X-TEOS (Fig. 4c) and Y-NaPMA (Fig. 4d) especially on the shell wall thickness of the NHSPs (Figs S14 and S15 †). Fig. 4c showed the decrease in shell-wall thickness (amorphous silica) from 40 nm (1.0 TEOS) down to 18 nm (0.4 TEOS) by reducing the X-TEOS concentrations. This proves that TEOS contributes the structural shell stability of the NHSPs due to the increase of shell thickness. While in Fig. 4d with increasing Y-NapMA concentrations, the observed average nano-size of the NHSPs was increased (Figs. 3d-II, 4b and 4d) but the shell-wall thickness remains unchanged (~18 nm–22 nm). This implied that NaPMA controlled the nano-size of the NHSPs. In the high-magnification-TEM images (Figs. 4c-III and 4d-III), an amorphous ultra–microporous morphology was highly visible as displayed on the surfaces of the silicate-shell wall of the NHSPs, even if the concentrations of X-TEOS and Y-NaPMA concentrations were varied and calcined (Figs. S14 and S15 †). To confirm the distinct property of the ultra-microporosity of the calcined-NHSPs, N_2 adsorption-desorption isotherms at 77 K using the BET method for surface area ($s.a_{BET}$) and DFT method for pore (space)-size distribution (PD) were carried out as shown in Fig. 5.

Mostly, the appearance of the isotherms for all the calcined-NHSPs samples (X-TEOS-C and Y-NaPMA-C) were almost the same which do not show any pronounced hysteresis and points towards the presence of (ultra)-micropores (present of steep slope in low p/p_o), mesopores of small diameter (shallow slope at intermediate p/p_o) and macropores[36,37] (Figs. 5a-I and

5b-I) which agreed with the TEM images as shown in Figs. 4c and 4d (Figs. S14 and S15 †).

All calcined-NHSPs samples showed an average s.a_{BET} ranging from ~85.3 m^2 g^{-1} to 54.1 m^2 g^{-1} and total pore volume ($V_{t\text{-}BJH}$) ranging from (~0.2–0.5) cc g^{-1}. In addition, the average pore-size distribution peak ranging from 7.56 nm to 10 nm was determined using DFT method based from the adsorption branch of the isotherm as shown in Figs. 5a-II and 5b-II (see also Tables S1–S5 †). This concludes the existence of the ultra-microporous morphologies on the shell surfaces of NHSPs, even though X-TEOS and Y-NaPMA were varied. This concurs with the images shown in Fig. 4 (Figs. S14 and S15 †).

However, higher s.a_{BET} was obtained as the concentrations of Y-NaPMA decreased as shown in Fig. 5b-I (Tables S3 and S4 †). This shows that nano-size of the NHSPs (see, also Fig. 4d and Fig. S15 †) is one of the key points in increasing the specific surface area (s.a_{BET}) even without adding any surfactant or changing the shell thickness and surface shell wall morphologies of the NHSPs.

In comparison, with decreasing X-TEOS, s.a_{BET} slightly increased as shown in Fig. 5a-I (Table S1 and S2 †). The slight increase in s.a_{BET} was caused by the thinning of the shell wall (amorphous silica shell wall) formed during the synthesis (Fig. 4c and Fig. S14 †). This means that nano-size and shell width can assist in altering the surface properties of the NHSPs.

To determine the average pore-size distribution, DFT analysis was used. Although the X-TEOS concentrations was varied, the average pore-size distribution remained constant (~10 nm) as shown in Fig. 5a-II (Figs S16-III, and S18-III †). With higher Y-NaPMA concentrations, the average pore-size distribution increased from 7.56 nm up to 17.99 nm as shown in Fig. 5b-II (Fig. S17-III and S19-III †). At this point, the presence of large pores around ~7.56 nm–17.99 nm was detected throughout the sorption measurements, mainly due to the integral presence of interstitial spacing between the hollow nanoparticles. This collaborated with the BJH analysis, which

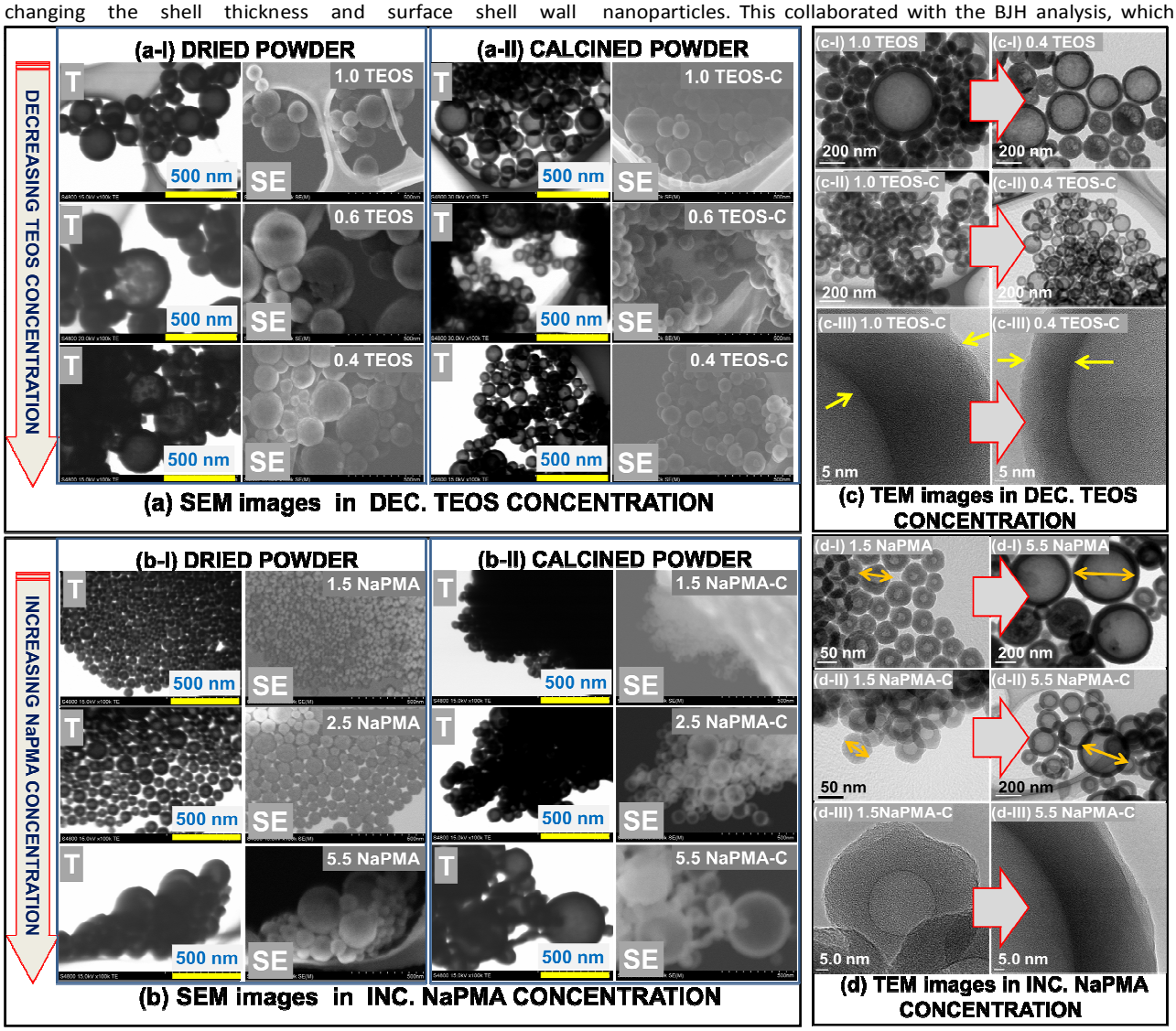

Fig. 4 (a, b) SEM images (transmission, T and secondary electron imaging mode, SE) of the (a-I, b-I) dried and (a-II, b-II) calcined powder of NHSPs in varying (a-I, a-II) X-TEOS and (b-I, b-II) Y-NaPMA concentrations. The (c, d) TEM images (c-III, d-III) high-magnification of (c-I, d-I) dried and (c-II, c-III, d-II, d-III) calcined-NHSPs samples with varying (c-I, c-II, c-III) X-TEOS and (d-I, d-II, d-III) Y-NaPMA concentrations.

yields broad range of pore sizes around 20 nm to 100 nm (Fig. S16-II to S19-II †).

From the TEM images with the support of the sorption isotherm including DFT and BJH analyses provided a strong indication for an amorphous disordered ultra-micropore structure with pore diameters of approximately less than 1.0 nm[37, 38] existed in the shell wall of the calcined–NHSPs.

We noted that the decrease in $s.a_{BET}$ after calcination of NHSPs was mainly due to the relaxation or slight sintering of the nano-silicate shell wall. This decreased the open pores in the surface shell (surface area) in between nano-silicate structure which support in stabilizing the shell-wall.[36] Eventually, this decreased the $V_{t\text{-}BJH}$ and micropore volumes (for complete data, Tables S1–S5 †). But, no major change in the XRD spectra (Figs. 3a and 3b) or TEM images (Figs. 4c and 4d) were observed.

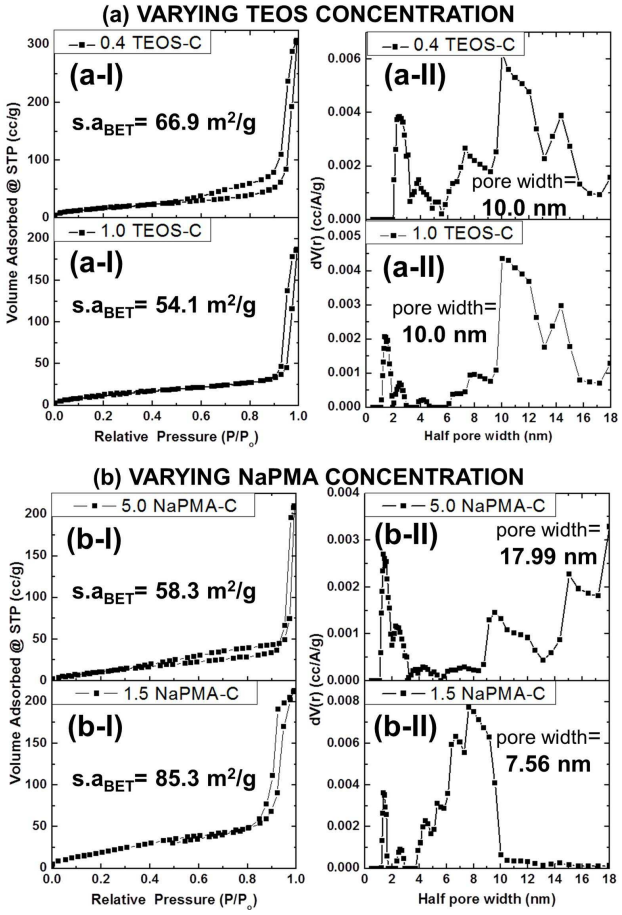

Fig. 5 (a-I, b-I) N_2 adsorption-desorption isotherm including surface area ($s.a_{BET}$) calculated by Brunauer-Emmett-Teller (BET) method with pore-size distribution calculated by (a-II, b-II) density functional theory (DFT) model of calcined-NHSPs samples with varying (a-I, a-II) X-TEOS-C and (b-I, b-II) Y-NaPMA-C concentrations.

Thermal conductivity of the glass substrate coated with NHSPs using the laser flash method

To validate initially the thermal-insulating property of the coated-glass with NHSPs, we used the 1.0 TEOS – NHSPs (ideal formula) as our NHSPs sample powder. The coated-glass with NHSPs was fabricated by sequential simple dip-coating process. Here, we varied the wt% solid concentrations and the number of dip coating in order to evaluate the thermal characteristic of coated-glass with NHSPs.

The thermal conductivity value of the coated-glass with NHSPs (k_{CG}) was calculated using equation 3. The summary of the results was seen in Table 1 and 2. The details about the xenon flash method can be seen from the corresponding references[19,30,32] for selected raw data's including the detailed schematic illustrations (Figs. S20, S22 and S23 †).

Based on the results, the k_{CG} containing 0.1 wt% solid concentrations (0.736 W m^{-1} K^{-1}) was decreased by about ~29.9% when compared with the plain glass substrate, 1.05 W m^{-1} K^{-1}, see Table 1 and Table S5 †. Based from actual results and referred references,[2,5,6] the reason for the reduced thermal conductivity was technically due to the hollow inner space of NHSPs present in coated-glass with NHSPs. The NHSPs helped reduce the thermal conduction due to phonon scattering.[6, 8] The ~29.9% decrease in thermal conductivity was quite significant, especially for thermal insulation of glass materials. But when NHSPs powder increased to 0.8 wt% solid concentrations, the thermal conductivity slightly increases (0.982 W m^{-1} K^{-1}, see Table 2) when compared to coated-glass with NHSPs containing 0.1 wt% solid concentrations (0.736 W m^{-1} K^{-1}). The increase in thermal conductivity was due the large amount of NHSPs that tends to aggregate and form conduction passages.[6,8] With this preliminary observations, NHSPs of adequate amount show mono-dispersion and act as insulating cells, whereas huge quantity of NHSPs tend to aggregate and form heat conduction passages resulting to higher thermal conductivities.[6]

Table 1 Thermal conductivity of coated-glass with NHSPs with 0.1% solid concentrations with varying dip coating

Sample material	Thermal conductivity (W m^{-1} K^{-1})	% difference compared to glass
glass substrate	1.05*	-
1.0 TEOS-0.1%-1x	0.78	25.6
1.0 TEOS 0.1%-6x	0.74	29.9

Table 2 Thermal conductivity of coated-glass with NHSPs in varying solid concentrations in one dipping

Sample material	Thermal conductivity (W m^{-1} K^{-1})	% difference compared to glass
glass substrate	1.05*	-
1.0 TEOS-0.81%-1x	0.98	6.50
1.0 TEOS-0.1%-1x	0.78	25.6

** thermal conductivity of glass given in reference[31]*

Relationship between transparency and thermal conductivity of the glass substrate coated with varying NHSPs.

In Fig. 6, we constructed a plot that revealed the relationship between the transparency and thermal conductivity of the glass substrate with varying weight percentage (wt %) of the solid concentration of NHSPs. As shown in Fig.6a, a decrease in

wt % of the solid concentration of NHSPs on the glass substrate surface was accompanied by a decrease in the thermal conductivity (k) of the sample material (determined using the Xenon flash method, Table 1 and 2).

The reduced thermal conductivity of the glass substrate with NHSPs was due to the hollow inner space of NHSPs that interrupted the heat flow across the glass substrate and trapped the heat flow inside the hollow space. But as the amount of NHSPs increased, the thermal conductivity increased which tend to behave similarly to the thermal conductivity of the (raw) glass. In this case, the (large) aggregate NHSPs tend to form a conduction passages.[2,5,6] The effect of transparency with varying amount of NHSPs on the glass substrate was checked and measured using UV/VIS/NIR spectrophotometer from the visible wavelength range (300 to 1000 nm, Fig.S26 and Fig. 6b). Here, the glass substrate with varying NHSPs wt% solid concentration (0.1% ~ 0.81%) and the reference clean glass substrate were prepared for transmittance measurement (single dip coating). As expected in Fig. 6b, the glass substrate with varying amount of NHSPs showed slight decrease in transparency (~ 800 nm wavelengths) but still retained a good transparency higher than 90 % even with increasing wt % of solid concentration of NHSPs. As clarified in the Fig. 6, increasing the wt % solid concentration of NHSPs on the surface of the glass substrate increased the thermal conductivity but the transparency of the sample slightly decreased.

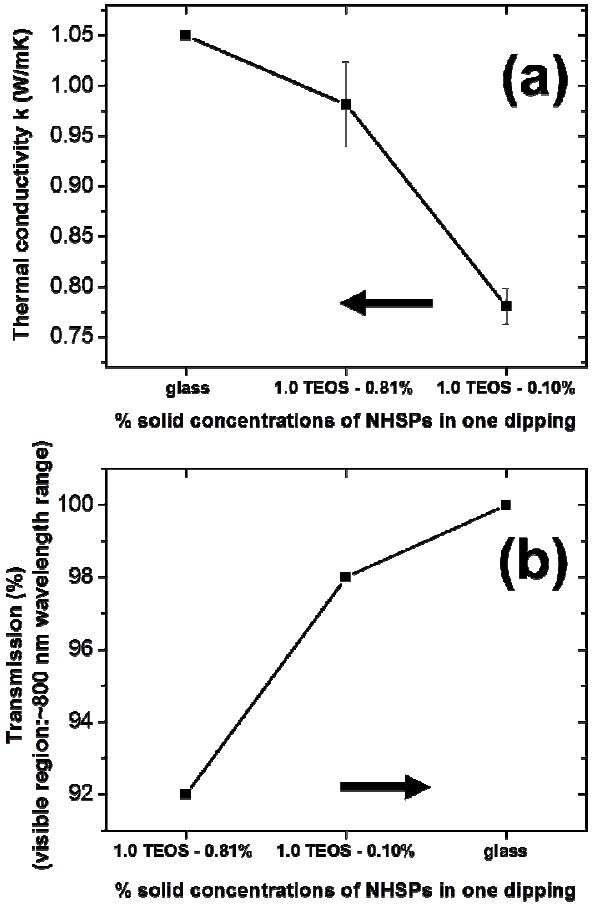

Fig. 6 Initial plots of the thermal conductivity (a) and light transmittance (b) at ~800 nm wavelength (visible range) of the glass substrate with varying weight percentage (wt %) of solid concentration of NHSPs for one dipping (one side only) using dip coater.

Conclusions

In summary, we have synthesized NHSPs by means of soluble soft-template method using the alternative-water soluble-NaPMA with TEOS via room temperature hydrolysis. Then, demonstrate the fabrication of coated-glass with NHSPs using the innovative dip coating approach. Flexibility in modifying the physico-chemical properties of NHSPs were demonstrated by tuning the formulated parameters such as the amount of TEOS and NaPMA concentrations. Under the present experimental conditions, variations of nano-size and shell thickness in NHSPs with ultra-microporous shells were made.

Here, we showed that with a sufficient amount of NHSPs coated onto the surface of glass substrate, transparent and thermally insulating materials was attained. This was partially due to the hollow inner nanosize-space present in NHSPs that helped interrupt the heat flow pass through the solid block material.

This approached lessen the multi-step procedure in investigating thermal insulation-property of NHSPs. Also, the innovative modification of NHSPs synthesis open up a promising route for the synthesis of other hybrid-inorganic materials with core-shell or hollow structures, as well as encapsulations of other oxide materials that will help improve the insulating properties of the hollow particles.

Moreover, we are able to show an alternative route in producing NHSPs at lower cost and enhanced environmentally friendly production route. We are also able to display the optimization of the nano-size dimensions (hollow nano-size and shell thickness) and develop simple approach in depositing the NHSPs onto glass substrate.

With these advantages, transparent and thermally insulating glass sheet with NHSPs was successfully demonstrated. Moreover, the fabrication of composite structural materials (aerogel materials with hybrid-hollow particles) is still ongoing.

Acknowledgements

This research was supported by Global Research Center for Environmental and Energy based on Nanomaterials Science (GREEN) at the National Institute for Materials Science (NIMS). We would like to express thanks to the technical support staff members (Makito Nakatsu, Kiyotaka Iiyama, Toshiaki Takei and Hidehiko Tanaka) of the International Center for Materials Nanoarchitectonics (MANA) at NIMS for assisting the authors with the used of analytical instruments.

Notes and references

‡ Note: (1) for comparison, the number of cycles of immersion was also varied from 1x to 6x; (2) To create a one side coating onto the glass substrate, during dip coat, the other side of the glass was covered with water-resistant tape, and then gently removed after drying in air.

‡‡ Note: for every measurement, all coated-glass with NHSPs samples were placed identically, 3.5 mm in front of the lamp, facing the light source is the side of the glass substrate with no coating (no NHSPs layers) but covered with black taped see, Figs. S3 and S4 † . The measurement was conducted in a controlled humidity and temperature condition.

‡‡‡ Note: Samples labelled with 1.0 TEOS or 4.0 NaPMA are actually the same specimen. They are labelled differently for the purpose of discussion. This is also the model reference formula for this paper.

1 X. W. Lou, L. A. Archer and Z. Yang, *Adv. Mater.*, 2008, **20**, 3987-4019.
2 F. Caruso, in *Colloid Chemistry II*, ed. M. Antonietti, Springer Berlin Heidelberg, 2003, pp. 145-168.
3 V. Valtchev and L. Tosheva, *Chem. Rev.*, 2013, **113**, 6734-6760.
4 X. Li, Y. Yang and Q. Yang, *J.Mater.Chem.A*, 2013, **1**, 1525-1535.
5 J. Gao, J. Wang, H. Xu and C. Wu, *Materials & Design*, 2013, **46**, 491-496.
6 M. Fuji and C. Takai, in *Nanoparticle Technology Handbook (Second Edition)*, ed. M. H. N. N. Yokoyama, Elsevier, Amsterdam, 2012, doi: http://dx.doi.org/10.1016/B978-0-444-56336-1.50072-2, pp. 679-684.
7 X. Y. Cui, N. Zhang, P. Y. Yao and B. Liang, 2012.
8 Y. Liao, X. Wu, Z. Wang, R. Yue, G. Liu and Y. Chen, *MCP*, 2012, **133**, 642-648.
9 T. Fiedler, H. S. Richards, I. V. Belova, A. Öchsner and G. E. Murch, *Exp. Therm Fluid Sci.*, 2013, **44**, 637-641.
10 Y. Zou, Y. Zhan, R. Zhao and X. Liu, *J Mater Sci: Mater Electron*, 2013, **24**, 1238-1242.
11 X. Lai, J. E. Halpert and D. Wang, *Energy Environ. Sci.*, 2012, **5**, 5604-5618.
12 R. Ghosh Chaudhuri and S. Paria, *Chem. Rev.*, 2011, **112**, 2373-2433.
13 Y. Liu, J. Goebl and Y. Yin, *Chem. Soc. Rev.*, 2013, **42**, 2610-2653.
14 J. Liu, F. Liu, K. Gao, J. Wu and D. Xue, *J. Mater. Chem.*, 2009, **19**, 6073-6084.
15 Y. Zhao and L. Jiang, *Adv. Mater.*, 2009, **21**, 3621-3638.
16 X. W. Lou, L. A. Archer and Z. Yang, *Adv. Mater.*, 2008, **20**, 3987-4019.
17 A. Guerrero-Martínez, J. Pérez-Juste and L. M. Liz-Marzán, *Adv. Mater.*, 2010, **22**, 1182-1195.
18 Y. Q. Cui and S. Riffat, *Applied Mechanics and Materials*, 2011, **71**, 1967-1970.
19 J. Blumm, A. Lindemann and S. Min, *Thermochim. Acta*, 2007, **455**, 26-29.
20 M. C. Stuart, R. de Vries and H. Lyklema, in *Fundamentals of Interface and Colloid Science*, ed. J. Lyklema, Academic Press, 2005, vol. Volume 5, pp. 1-84.
21 B. Du, Z. Cao, Z. Li, A. Mei, X. Zhang, J. Nie, J. Xu and Z. Fan, *Langmuir*, 2009, **25**, 12367-12373.
22 H. Woo and K. Char, *Macromolecular Research*, 2013, **21**, 1004-1010.
23 Y. Wan and S.-H. Yu, *J. Phys. Chem. C*, 2008, **112**, 3641-3647.
24 V. Masalov, N. Sukhinina, E. Kudrenko and G. Emelchenko, *Nanotechnology*, 2011, **22**, 275718.
25 Y. Du, L. E. Luna, W. S. Tan, M. F. Rubner and R. E. Cohen, *ACS Nano*, 2010, **4**, 4308-4316.
26 M. D'Acunzi, L. Mammen, M. Singh, X. Deng, M. Roth, G. K. Auernhammer, H.-J. Butt and D. Vollmer, *Faraday Discuss.*, 2010, **146**, 35-48.
27 K. S. W. Sing, D. H. Everett, R. A. W. Haul, L. Moscou, R. A. Pierotti, J. Rouquerol and T. Siemieniewska, in *Handbook of Heterogeneous Catalysis*, Wiley-VCH Verlag GmbH & Co. KGaA, 2008, DOI: 10.1002/9783527610044.hetcat0065.
28 E. P. Barrett, L. G. Joyner and P. P. Halenda, *J Am Chem Soc*, 1951, **73**, 373-380.
29 P. I. Ravikovitch and A. V. Neimark, *J. Phys. Chem. B*, 2001, **105**, 6817-6823.
30 S.-K. Kim and Y.-J. Kim, *Thermochim. Acta*, 2008, **468**, 6-9.
31 F. P. Incropera, *Fundamentals of heat and mass transfer*, John Wiley, 2007.
32 L. Matthews, R. Viskanta and F. Incropera, *IJHMT*, 1984, **27**, 487-495.
33 K. Kamitsuji, S. Ueno, H. Suzuki, Y. Kimura, T. Sato, T. Tanigaki, O. Kido, M. Kurumada and C. Kaito, *A&A*, 2004, **422**, 975-979.
34 T. Thanh Nhan, P. Thi Van Anh, L. My Loan Phung, N. Thi Phuong Thoa and T. Van Man, *Adv. Nat. Sci: Nanosci. Nanotechnol.*, 2013, **4**, 045007.
35 Z.-Z. Li, L.-X. Wen, L. Shao and J.-F. Chen, *J. Controlled Release*, 2004, **98**, 245-254.
36 P. Ruckdeschel, T. W. Kemnitzer, F. A. Nutz, J. Senker and M. Retsch, *Nanoscale*, 2015, **7**, 10059-10070.
37 T. Miyao, K. Minoshima, Y. Kurokawa, K. Shinohara, W. Shen and S. Naito, *Catal. Today*, 2008, **132**, 132-137.
38 N. C. Strandwitz and G. D. Stucky, *Chem. Mater.*, 2009, **21**, 4577-4582.

Synthesis and characterization of geometrically tunable nano-size hollow silicate particles and their dip-coating prepared films for thermal management applications

Raymond V.Rivera Virtudazo[a], Ye Lin[b], and Rudder T. Wu*[c]

[a]*Global Research Center for Environment and Energy Based on Nanomaterials Science (GREEN), National Institute for Materials Science (NIMS), Namiki, Tsukuba, Ibaraki 305-0044 Japan*

[b]*School of Municipal and Environmental Engineering, Shenyang Jianzhu University, Shenyang China*

[c]*National Institute for Materials Science (NIMS), Tsukuba, Ibaraki 305-0044 Japan*

*corresponding author. TEL: +81-(0)29-860-4702 FAX: +81-(0)29-860-4984
*E-mail: WU.rudder@nims.go.jp

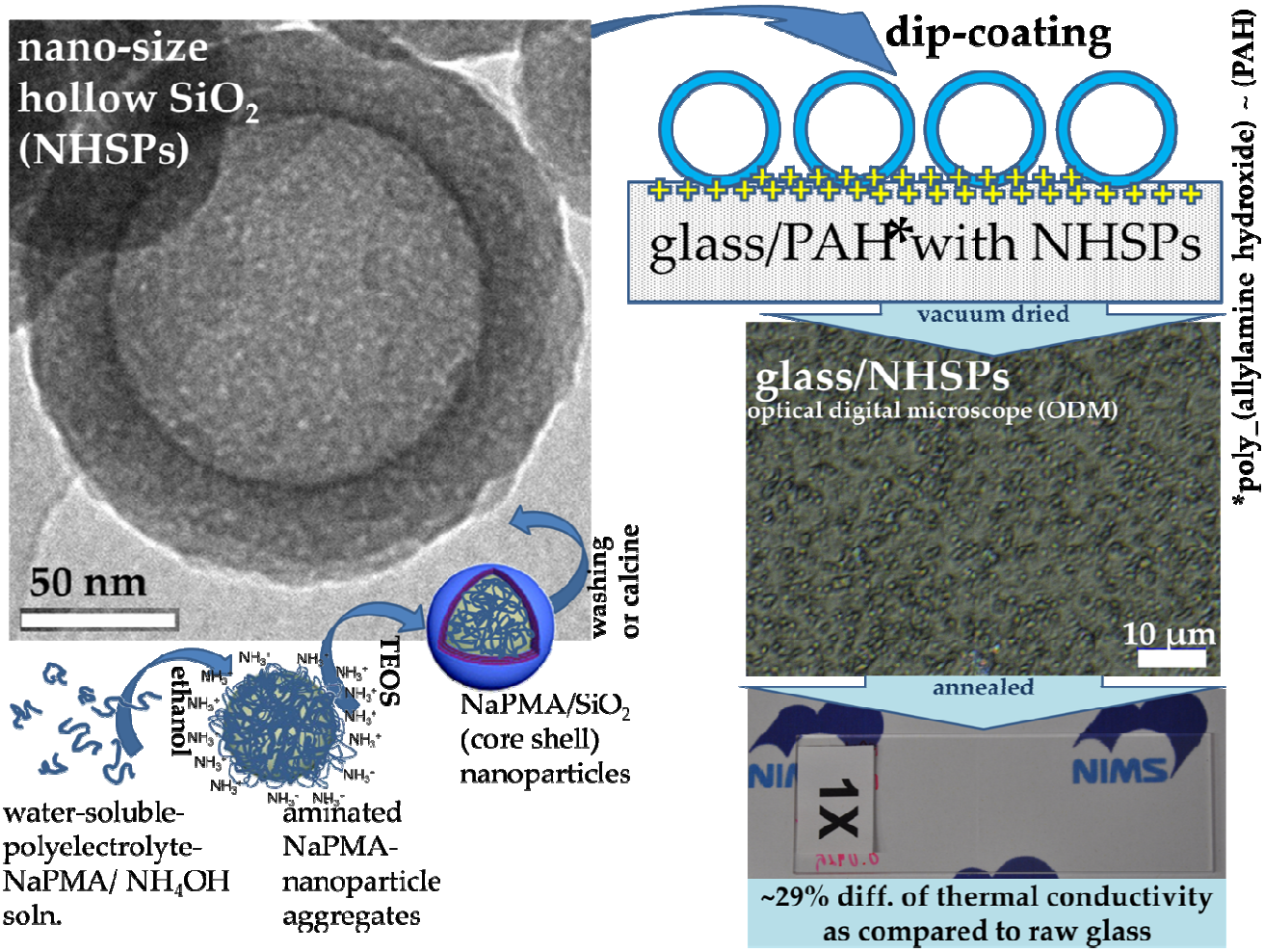

The thermal insulating feature of nano-size hollow silicate particles (NHSPs) was demonstrated by coating the glass substrate with NHSPs, a reduction of approximately 29.9 % in thermal conductivity was observed after coating the glass substrate, which was evaluated by a contactless approach using the xenon flash lamp set-up.